IN-02-CR
110989
29P.

DEVELOPMENT AND APPLICATION OF COMPUTATIONAL AEROTHERMODYNAMICS FLOWFIELD COMPUTER CODES

Technical Progress Report

for
Cooperative Agreement No. NCC2-420

for the period
September 1, 1986 - October 31, 1987

Submitted to

National Aeronautics and Space Administration
Ames Research Center
Moffett Field, California 94035

Aerothermodynamics Branch
Dr. George S. Deiwert, Chief and Technical Monitor

Thermosciences Division
Dr. Jim Arnold, Chief

Prepared by

ELORET INSTITUTE
1178 Maraschino Drive
Sunnyvale, CA 94087
Phone: 408 730-8422 and 415 493-4710
Telex: 62 44 2780
K. Heinemann, President and Grant Administrator
Ethiraj Venkatapathy, Principal Investigator

9 December, 1987

(NASA-CR-181534) DEVELOPMENT AND APPLICATION OF COMPUTATIONAL AEROTHERMODYNAMICS FLOWFIELD COMPUTER CODES Technical Progress Report, 1 Sep. 1986 - 31 Oct. 1987 (Eloret Corp.) 29 p CSCL 01A G3/02 N88-12465 Unclas 0110989

IN-02-CR
110989
29P.

DEVELOPMENT AND APPLICATION OF COMPUTATIONAL AEROTHERMODYNAMICS FLOWFIELD COMPUTER CODES

Technical Progress Report

for
Cooperative Agreement No. NCC2-420

for the period
September 1, 1986 - October 31, 1987

Submitted to

National Aeronautics and Space Administration
Ames Research Center
Moffett Field, California 94035

Aerothermodynamics Branch
Dr. George S. Deiwert, Chief and Technical Monitor

Thermosciences Division
Dr. Jim Arnold, Chief

Prepared by

ELORET INSTITUTE
1178 Maraschino Drive
Sunnyvale, CA 94087
Phone: 408 730-8422 and 415 493-4710
Telex: 62 44 2780
K. Heinemann, President and Grant Administrator
Ethiraj Venkatapathy, Principal Investigator

9 December, 1987

(NASA-CR-181534) DEVELOPMENT AND APPLICATION OF COMPUTATIONAL AEROTHERMODYNAMICS FLOWFIELD COMPUTER CODES Technical Progress Report, 1 Sep. 1986 - 31 Oct. 1987 (Eloret Corp.) 29 p CSCL 01A G3/02 N88-12465 Unclas 0110989

Summary

In the present work, multiple nozzle plume flow field is computed with a 3-D, Navier-Stokes solver. Numerical simulation is performed with a flux-split, two-factor, time asymptotic viscous flow solver of Ying and Steger. The two factor splitting provides a stable 3-D solution procedure under ideal-gas assumptions. An ad-hoc acceleration procedure that shows promise in improving the convergence rate by a factor of three for steady state problems is utilized. Computed solutions to generic problems at various altitude and flight conditions show flow field complexity and three-dimensional effects due to multiple nozzle jet interactions. Viscous, ideal gas solutions for the symmetric nozzle are compared with other numerical solutions.

Introduction

Supersonic and hypersonic vehicles, such as single- and multi-stage rockets, National Aerospace plane, Aeroassisted Orbital Transfer vehicles etc., incorporate integrated propulsion systems. The flight characteristics and the aerodynamic and propulsive efficiencies of these aerospace vehicles depend on ideal development of the the exhaust/plume flow field in the aft section of the body. If the vehicle design involves integration of aerodynamics and propulsion systems, (such as the NASP), then clear understanding of the plume flow field throughout the flight domain becomes very essential for accurate design and efficient operation.

The hypervelocity, high altitude plume flows are dominated by inviscid flow phenomenon, viscous-inviscid interactions and viscous-

viscous interactions. The occurrance of stationary barrel shocks, mach discs and shear layer-shock interactions are some unique flow features found in plume flows. The plume flow field may develop to be highly three dimensional, depending on the vehicle geometry and flight conditions. Due to high velocity and temperature, the gaseous mixture can react to form new species and the chemical reactions will influence the flow significantly. The combustion products, burned and unburned gaseous mixtures, may further react with the external gas mixture in the plume region. The chemically reacting flow field will differ significantly from ideal or non-reacting flows. Hence numerical procedures for the plume flow problems should be capable of addressing all these issues accurately. To reach this goal, first , 3-d, ideal-gas solutions are computed to explore the accuracy and stability of 3-d, Navier-Stokes solver. A reacting flow code will be built based on the experience gained with the ideal-gas solver.

Significant advances have been made in recent years to compute solutions to Euler and Navier-Stokes equations [1,2,3,4,5,6,7] in multi-dimensions. Advances made to extend method of characteristics to systems of equations in the form of flux splitting and differencing [2,3,5,6,7] schemes have proved very successful. To eliminate non-physi-cal solutions and to capture shocks with minimal shock dissipation various switch operators and Total Variation Diminishing (TVD) schemes[8] have been proposed and used. Stability and efficiency of three-dimensional solvers also have improved significantly in the recent years due to proper operator splittings and LU decomposition schemes coupled with upwind differencing.

In the present work, the two-factored flux-split scheme (TFS) of Ying and Steger [6,9] is applied to supersonic plume flows. The TFS scheme is unconditionally stable and convergent for linear systems of equations. Numerical experiments and solutions to transonic flows showed strong stability and accuracy for three dimensional flows[9]. Though the method does not have any limitations for supersonic and hypersonic flows, the application to plume flows is one of the attempts in establishing the accuracy and applicability of the TFS solver to supersonic and hypersonic flows.

Two-factor Flux Split Scheme for Navier Stokes Equations

Efforts in the past to extend two-dimensional solvers to three-dimensions have met with mixed success. Extending two-dimensional flow solver to three-dimensions is not conceptually difficult except for stability and convergence. As an example, the Beam and Warming ADI splitting[1] and LU (lower-Upper triangular matrix) factorization schemes [10] have proved to be neutrally stable in three-dimensions, (while such methods are unconditionally stable in two dimension) requiring artificial viscosity to be added to enhance the stability. On the other hand, schemes based on method of characteristics or upwind methods have been easier to extend from two- to three-dimensions and the stability of upwind schemes have not deteriorated with added dimension. Upwind methods have also yielded a variety of solution techniques due to positive and negative flux splitting or differencing, such as 2- ,3- or n-factor schemes[2,3,6], and relaxation procedures[7,11].

In 1986, Ying and Steger [6,9] proposed a two-factor flux split

(TFS) scheme for the solution of thin-layer, Navier-Stokes equations in three-dimensions. The TFS scheme is second order accurate in space and first or second order accurate in time. The scheme has been proven to be unconditionally stable[9] for linear three-dimensional model problems and numerical experiments confirm strong stability for three-dimensional Navier-Stokes problems. The flux splitting and transition operators allow strong normal shocks (normal to the flux split direction) to be captured with minimal dissipation and oscillation. Due to its strong stability, steady state solutions can be achieved quickly with large Courant numbers and with the use of local time steps.

TFS scheme has been validated for three-dimensional inviscid and laminar flows over simple configurations at transonic and subsonic speeds by Ying and Steger[6,9]. Rizk[12] applied the TFS scheme to external hypersonic flow around complex lifting bodies. In the present work TFS scheme is applied to plume flows. Only a limited insight into the TFS scheme is provided here and interested readers will find full detail in Ref. 9.

The Navier-Stokes equations with thin-layer approximation, in three-dimension and in generalized coordinates can be written as :

$$\frac{\partial \hat{Q}}{\partial t} + \frac{\partial \hat{E}}{\partial \xi} + \frac{\partial \hat{F}}{\partial \eta} + \frac{\partial \hat{G}}{\partial \varsigma} = Re^{-1}\frac{\partial \hat{S}}{\partial \varsigma} \tag{1}$$

where the conservative variable $\hat{Q}$ is,

$$\hat{Q} = J^{-1}\{\rho, \rho u, \rho v, \rho w, e\}^T$$

and the inviscid fluxes are,

$$\hat{E} = J^{-1}\{\rho U, \rho u U + \xi_x p, \rho v U + \xi_y p, \rho w U + \xi_z p, (e+p)U - \xi_t p, \}^T \quad (3)$$

$$\hat{F} = J^{-1}\{\rho V, \rho u V + \eta_x p, \rho v V + \eta_y p, \rho w V + \eta_z p, (e+p)V - \eta_t p, \}^T \quad (4)$$

$$\hat{F} = J^{-1}\{\rho V, \rho u V + \eta_x p, \rho v V + \eta_y p, \rho w V + \eta_z p, (e+p)V - \eta_t p, \}^T \quad (5)$$

$$\hat{G} = J^{-1}\{\rho W, \rho u W + \varsigma_x p, \rho v W + \varsigma_y p, \rho w W + \varsigma_z p, (e+p)W - \varsigma_t p, \}^T \quad (6)$$

In the above equations p is the pressure, and e is the total energy, and they are related as follows.

$$p = (\gamma - 1)[e - 0.5\rho(u^2 + v^2 + w^2)] \quad (7)$$

The scalar variable J is the Jacobian of the transformation and U, V and W are the contravariant velocity components along ξ, η and ς coordinate directions. The generalized coordinate variables ξ, η and ς are functions of the cartesian coordinates. Following Steger and Warming, a brief description of the flux splitting is given.

The fluxes along the generalized coordinate directions , $\hat{E}$, $\hat{F}$ and $\hat{G}$ can be split based on positive and negative eigenvalues along the respective coordinate directions since they are homogeneous functions of degree one in $\hat{Q}$. The homogeneous property allows one to write $\hat{E}$ as

$$\hat{E} = \hat{A}\hat{Q} = R\Lambda R^{-1}\hat{Q} \quad (8)$$

where $\hat{A}$ is the true flux Jacobian matrix associated with $\hat{E}$, and Λ is the diagonal matrix of eigenvalues, and R and R^{-1} are the right and left eigenvector matrices. The eigenvalues can be split into positive and negative components and the above equation can be expressed as

$$\hat{E}^{\pm} = R\Lambda^{\pm}R^{-1}\hat{Q} = \hat{A}^{\pm}\hat{Q} \tag{9}$$

This allows one to rewrite the flux $\hat{E}$ into

$$\hat{E} = \hat{E}^{+} + \hat{E}^{-} \tag{10}$$

where $\hat{E}^{+}$ and $\hat{E}^{-}$ are the split fluxes based on eigenvalues. Another way to express the split fluxes is to rewrite the flux vector in terms of the eigenvalues of the Jacobian matrix as below.

$$\hat{E} = \hat{E}_1 + \hat{E}_4 + \hat{E}_5 \tag{11}$$

where the split fluxes $\hat{E}_1$, $\hat{E}_4$, $\hat{E}_5$ correspond to the three distinct eigenvalues[13]

The positive and negative fluxes are computed directly from the equation (11) by substituting $\Lambda = \Lambda^{+}$ or $\Lambda = \Lambda^{-}$ respectively. The above Steger-Warming[13] flux splitting then allows proper differencing of spatial derivatives based on local eigenvalues and the resulting difference scheme can be cast into a two factor form.

In the TFS scheme of Ying and Steger, the flux vector splitting is applied only to the fluxes along the ξ direction. The fluxes along the other two coordinate direction are not split and centered differences are used to approximate the spatial inviscid and viscous flux terms. The splitting of the streamwise flux terms permits a two factor difference scheme to be formed as shown below.

$$\left(I+\theta\Delta t\mathcal{L}^{+}\right)\left(I+\theta\Delta t\mathcal{L}^{-}\right)\Delta\hat{Q}^{n}=RHS \tag{12}$$

where

$$RHS=-\Delta t\left[\delta_{\xi}^{b}\hat{E}^{+n}+\delta_{\xi}^{f}\hat{E}^{-n}+\delta_{\eta}^{c}\hat{F}^{n}+\delta_{\varsigma}^{c}\hat{G}^{n}-Re^{-1}\bar{\delta}_{\varsigma}\hat{S}^{n}-D_{e}\hat{Q}^{n}\right] \tag{13}$$

$$\mathcal{L}^{+}=\delta_{\xi}^{b}\hat{A}^{+n}+\delta_{\varsigma}^{c}\hat{C}^{n}-Re^{-1}\bar{\delta}_{\varsigma}\left(J^{-1}\hat{M}J\right)-D_{i\xi} \tag{14}$$

$$\mathcal{L}^{-}=\delta_{\xi}^{f}\hat{A}^{-n}+\delta_{\eta}^{c}\hat{B}^{n}-D_{i\eta} \tag{15}$$

For a full explanation of all the terms see Reference 9. The left hand side of the above algorithm consists of two operators. The operator $\left(I+\theta\Delta t\mathcal{L}^{+}\right)$ is block lower triangular (in ξ), block tridiagonal (in ς) matrix containing a second order backward differences in ξ direction and central differences in the ς direction. Similarly, the second operator $\left(I+\theta\Delta t\mathcal{L}^{-}\right)$ is a block upper triangular (in ξ), block tridiagonal (in η) matrix containing a second order differences in ξ direction and central differences in the η direction. By inverting the two block operators by a series of block tridiagonal inversions, one solves for the changes in the conservative variables between time level (n) and $(n+1)$. Coupled to the above solution procedure, appropriate explicit boundary conditions are applied to compute the conservative variable along the boundary surfaces.

The above procedure can be either first- or second-order accurate in time and second order accurate in space. Due to two-factor flux splitting, improved stability is achieved compared to central

differenced, three factor schemes. To avoid non-physical solutions limiters defined in Ref.9 are used to limit the spread and oscillation of shocks.

Plume Flow Problems

The plume flow problem can be characterized by the interaction between single or multiple jets and supersonic or subsonic outer-flows. A schematic of the plume flow is given in Figure 1. The high altitude, hypervelocity outer flow, complicated by the three dimensional body shape interacting with multiple jet streams result in barrel shocks, Mach discs, mixing shear layers and recompression shocks. The numerical solver should be capable of predicting all the flow features accurately in the chemically reacting environment. As a first step in evolving a three-dimensional reacting flow solver, the ideal gas plume flow problem is addressed with the TFS method.

The TFS solver is first applied to an axisymmetric plume flow problem for validation purposes. The first problem solved is an AGARD test case for which both experimental[14] and numerical results[15] are available. This flow involved a single sharp-lipped nozzle jet interacting with an external supersonic flow behind a 5° conical after body. The free stream Mach number was 2.2 and the jet-exit Mach number was 2.024. The jet-exit to free-stream pressure ratio was 1.370. Since the external and the nozzle jet-exit flow were supersonic, the fore body was not included in the present computations and this simplified the grid used in the present computation. The effect of fore body and nozzle upstream flow were introduced only through the inflow boundary conditions. Figure 2. shows the three

dimensional grid (61x10x61) used in the present computation. The TFS solver was able to compute the flow without any numerical difficulty and the steady state solution was achieved within 1500 steps. No turbulence viscosity was included. The general plume flow features observed in Ref. 15. are captured well in the present results. The pressure contours in the plume region are shown in Figure 3. The external compression shock, the formation of a weak barrel shock and its reflection, and the mixing shear layer can be seen from the pressure contours plot. Mach number and temperature comparisons between the present result and that of Deiwert, et. al [15] are shown in Figures 4 and 5.. The TFS results agree reasonably well even though the hard body and turbulence effects were neglected in the present computations.

Next , a three-dimensional plume flow around a generic rocket is considered. The generic rocket consists of a blunt fore-body followed by an axisymmetric mid-section. The aft section of the body consists of two-nozzles projecting out of the base region. Figure 6. shows the the body and the nozzles shape. Even at zero degree angle of attack, the external flow field is axisymmetric only around the fore- and mid-body regions. The multiple nozzles make the flow three-dimensional in the aft section and the plume flow can only be solved with a three-dimensional solver. The computational domain, as before, is limited to the plume region. An example three-dimensional physical grid is shown in Figure 7. The flow is symmetric about the yx-plane and zx-plane and so the computational plane can be limited to one quadrant as shown. To impose nozzle exit conditions accurately, the physical grid was constructed in patches,

taking advantage of the local topology. The grid in a ξ constant plane is shown in Figure 8.. Notice the grid is nearly cylindrical around the nozzle centerline. A grid singularity exists along $\varsigma = 0$ plane, but does not present any problem in the present computations. All the boundary conditions were applied explicitly and they are free stream conditions along $\varsigma = 1.0$ and z-symmetry along $\eta = 0$ plane and part z-symmetry and part y-symmetry along $\eta = 1.0$ plane. Along $\xi = 0$ plane (inflow) free stream conditions are applied external to the nozzle region and nozzle exit plane conditions are applied in the nozzle region. A conical nozzle with 11.4 deg. half cone angle was assumed in computing the nozzle exit-plane conditions. Simple extrapolation was used along ξ=1.0 plane (outflow). Along the singular plane (ς=0.0) an extrapolated averaging was used.

Solutions for three different flow conditions corresponding to three different altitude were computed and are presented here. Free stream conditions for the three test cases are listed in the following table.

Case	Alt.	Velocity	Mach No.	Temp.	Press.
	km	m/s		K	atm
1	15	542	1.84	217	0.120
2	30	1022	3.39	226	0.013
3	45	1341	4.22	250	0.0028

and the nozzle exit conditions for all the cases are:

$$\begin{aligned} \text{Temperature} &= 2000 \quad K \\ \text{Pressure} &= 1 \quad atm. \\ \text{Velocity} &= 2767 \quad m/sec \end{aligned}$$

Various numerical tests and improvements were performed in computing these test cases with the TFS solver. Solutions in all cases

were obtained under laminar flow conditions and no turbulent viscosity was used. Work is in progress to include the fore-body geometry and algebraic turbulence models. Solutions to all three test cases are given next.

Numerical Solutions : Test case 1

The free stream and the nozzle exit conditions for this test case corresponds to an altitude of 15 Km. An example grid (95x25x47) used in discretizing the physical domain is shown in Figure 7 and it shows the grid lines along the symmetry plane and at the out-flow plane. Along constant ξ plane, the grids are similar to the grid along the out-flow plane. This grid was developed in patches and assembled. With known inflow conditions, a steady state solution was obtained in 2000 iterations with no computational difficulty. The converged solution in terms of normalized pressure and Mach number contours are shown in Figures 9 and 10 respectively. The outflow plane is at 140m downstream of the jet-exit plane and the outer boundary is 20m away from the x-axis. The numerical results clearly show the following features. The flow is three-dimensional and the shear-layer spread rate is different along the symmetry planes. The under-expanded jet accelarates and the expansion causes the pressure and temperature to drop rapidly downstream of the nozzle exit plane. The external flow is compressed by the lip-shock. A shear layer emanates from the edge of the nozzle. As the shear layer is turned towards the axis, a barrel shocks forms inside the shear layer region. Due to three-dimensionality, this barrel shock is non-symmetric and it converges towards the axis to form a Mach disc (due to poor grid res-

olution, the present solution does not show a mach disc, but only a reflection), and the expanding central core of the jet is compressed suddenly. The pressure and the temperature rises behind the shock reflection point and the reflected shock interacts with the jet shear layer. The repeated deflection of the shear layer and the formation and reflection of barrel shocks are visible from the contour plots. Variation of pressure, density and Mach number along X-axis are shown in Figures 11, 12 and 13. These plots show, at least, two Mach discs/shock reflection points along the axis. To obtain better shock reflection along the x-axis, an one dimensional adaptation was performed on one of the grids and Mach contours from the adapted grid solution are shown in Figure 14. The shock reflection is resolved well and better distribution of the grid points improved the overall solution. From these numerical solutions, we observe the following. For this test case, the first shock reflection occurs around 14.5m downstream of the exit plane and the second reflection is observed around 33 m. Maximum Mach number of 6.95 is reached just ahead of the Mach reflection point and the maximum temperature reached is 1400 K, behind the first shock reflection point. An interesting observation is that the mixing shear layer does not spread away from the x-axis. Instead, it is centered around the axis and reaches an asymptotic size in the far-field downstream of the exit plane. The maximum cross section of the shear layer occurs upstream of the first reflection point. Also, the plume flow remains three dimensional even in the far field region.

Numerical Solutions : Test case 2

Next set of solutions presented correspond to the second case conditions shown in Table 1. The grid used in the present computations are the same as previous case (Figure 7). The jet exit conditions are more under-expanded compared to the previous case due to decrease in external pressure (higher altitude) and this resulted in rapid expansion and stronger flow structures in the plume region. The pressure and Mach number contour plots are shown in Figures 15 and 16. The flow development and the flow features are similar to the previous case. The first shock reflection is observed at 42m downstream of the exit plane and the second reflection is at 95m (pressure contours). The non-axisymmetry of the flow starts right near the jet exit plane due to inflow conditions being non-symmetric and the Mach number contours along the z-symmetry plane and y-symmetry plane show the three-dimensionality of the flow. The maximum Mach number reached is 13.5 and the temperature rises to 1100 K behind the first shock reflection point.

Numerical Solutions : Test case 3

Numerical solutions to the third test case, corresponding to an altitude of 45 Km is given next. The grid used is the same as in previous cases. The numerical solver experienced some difficulty with very high local Courant numbers and with lower Courant number, the severely under-expanded jet conditions required more iterations to converge towards the steady state. The maximum allowable local Courant number was considerably smaller than the previous two cases.

The converged solution is presented in terms of pressure and Mach number contours in Figures 17 and 18. The highly energetic under expanded jet continued to accelerate until the shock reflection point which is at 75m downstream of the nozzle exit plane. The flow is considerably more three dimensional compared to the previous two cases and shear layer spread rate along the two planes of symmetry differ greatly.

Though the nozzle exit conditions remain the same between the three cases, the altitude variation caused the jet exit conditions to be highly under-expanded at higher altitude. The increased jet exit to external pressure ratio resulted in high acceleration in the plume region and each of the barrel shocks and the shock reflection points occur further downstream. The pressure, temperature, density and Mach number variation along the x-axis, down stream of the exit plane, for the last two cases are shown in Figure 19, 20, 21 and 22. From these, we observe the following. The pressure rise after the first shock is nearly the same in all cases. The maximum Mach number reached ahead and the peak temperature behind the Mach reflection depend on the free-stream conditions.

Concluding Remarks

The two factor, flux split scheme of Ying and Steger is applied to three-dimensional supersonic plume flows. The numerical solutions to the axisymmetric test problem compares favorable well with other numerical solution. The TFS scheme predicted the complex flow structure well for the plume flows. TFS scheme is found to be stable and in most cases, a steady state converged solution is obtained

within 2000 time steps. The computed solutions exhibit flow structure that are physical and three-dimensional in nature. The numerical solutions gave greater insight into the development of the two-nozzle plume flow.

Presently efforts are underway to add the effect of the forebody in our computations. To accomodate the complex aft body region, multiple overlapping grids and the associated data management schemes are being added to the flow solver. Steady state accelaration procedures, such as simple variations of multigrid methods are being explored. Efforts are underway to modify the solver for computing equilibrium and non-equilibrium flows.

References

1. Pulliam, T. H. and Steger, J. L. '' On Implicit Finite-Difference Simulation of Three-dimensional Flows,'' AIAA Paper 78--10.

2. Bunning, P. G. and Steger, J. L. '' Solution of Two-Dimensional Euler Equations with Generalized Coordinate Transformation Using Flux Vector Splitting,'' AIAA Paper 82--0971.

3. Chakravarthi, S. R. and Szema, K. Y. '' An Euler Solver for Three-Dimensional Supersonic Flows with Subsonic Pockets,'' AIAA Paper 85-1703,1985.

4. Pulliam, T. H. and Steger, J. L. '' Recent Improvements in Efficiency, Accuracy, and Convergence for Implicit Approximate Factorization Algorithms,'' AIAA Paper 85--0360.

5. Anderson, W. K., Thomas, J. L. and Van Leer, B. '' A Comparison of Finite Volume Flux Vector Splittings for the Euler Equations,'' AIAA Paper No. 85--0122.

6. Ying, S.X., Steger, J. L. , Schiff, L. B. and Baganoff, D. "Numerical Simulation of Unsteady, Viscous, High Angle of Attack Flows Using a Partially Flux Split Algorithm,'' AIAA Paper 86-2179, 1986.

7. Bardina, J. and Lombard C. K. '' Three-Dimensional Hypersonic Flow Simulations with the CSCM Implicit Upwind Navier-Stokes Method,'' AIAA Paper 87-1114-CP.

8. Yee, H. '' Construction of explicit and Implicit symmetric TVD schemes and their Applications,'' *Journal of Computational Physics*, vol. 68, 1987.

9. Ying, S. X. '' Three-Dimensional Implicit Approximately Factored Schemes for Equations in Gasdynamics,'' Ph.D. Thesis, Stanford University, 1986.

10. Fujii, K. and Obayashi, S. '' Practical Applications of New LU-ADI SCheme for Three-Dimensional Navier-Stokes Computation of Transonic Viscous Flows,'' AIAA Paper 86-0513.

11. Yoon, S. and Jameson, A. '' An LU-SSOR Scheme for the Euler and Navier-Stokes Equations,'' AIAA Paper 87-0600.

12. Rizk, Y. Chaussee, D. and Steger, J. L. '' Numerical Simulation of the Hypersonic Flow Around Lifting Vehicles,'' NASA TM 89444, 1987.

13. Steger, J, L. and Warming, R. F. '' Flux Vector Splitting of the Inviscid Gasdynamic Equations with Applications to FInite Difference Methods,'' *J. Computational Physics, Vol. 40, No.2.*

14. AGARD Advisory Report No. 226, '' Report of the Working Group on Aerodynamics of Afterbody,'' June 1986.

15. Deiwert, G. S., Andrews, A. E. and Nakahashi, K. '' Theoretical Analysis of Aircraft Afterbody Flow,'' AIAA Paper 84-1524.

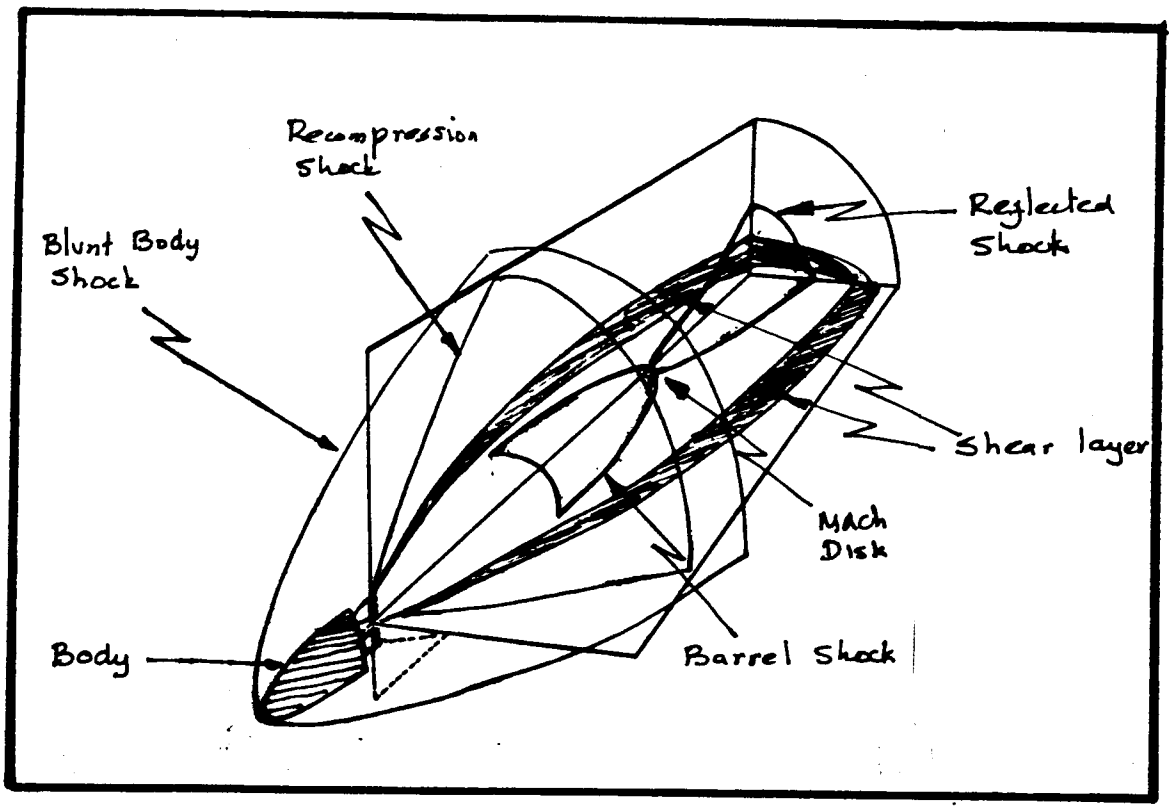

Figure 1. A Three-Dimensional Schematic of the Plume Region.

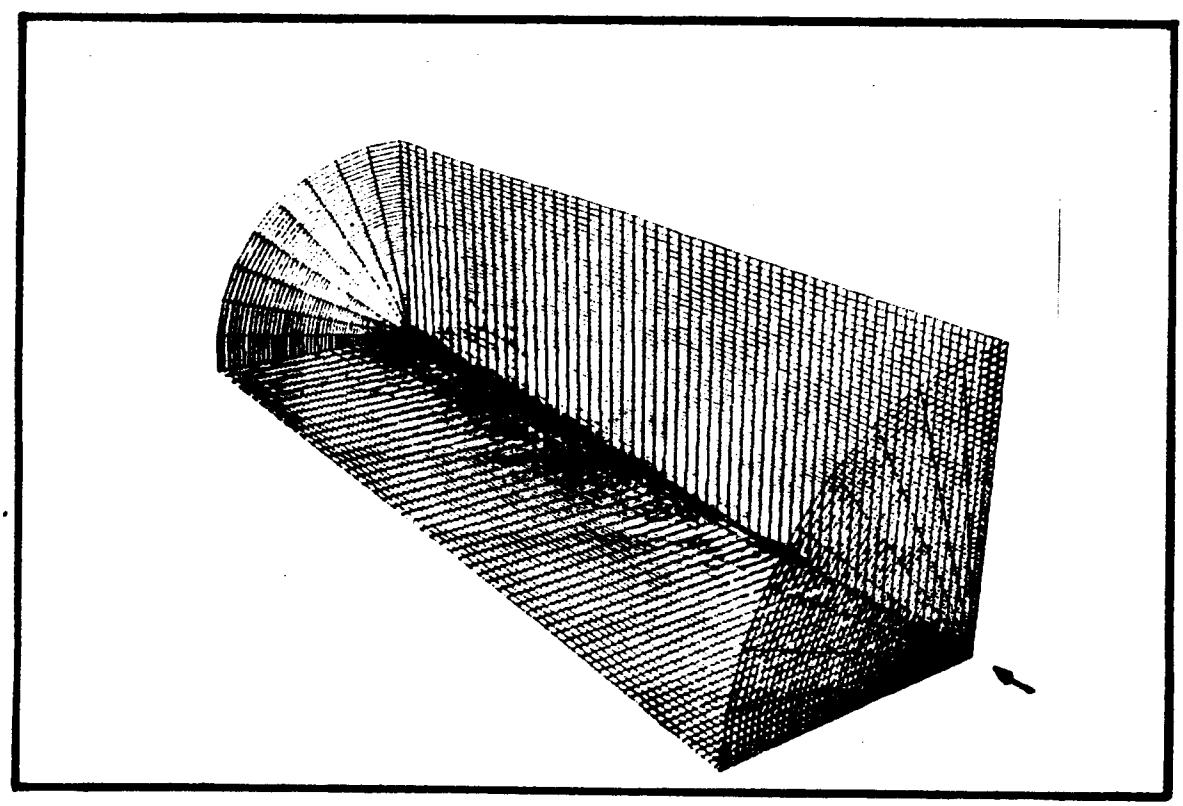

Figure 2. 3-D Grid for AGARD Test Case.

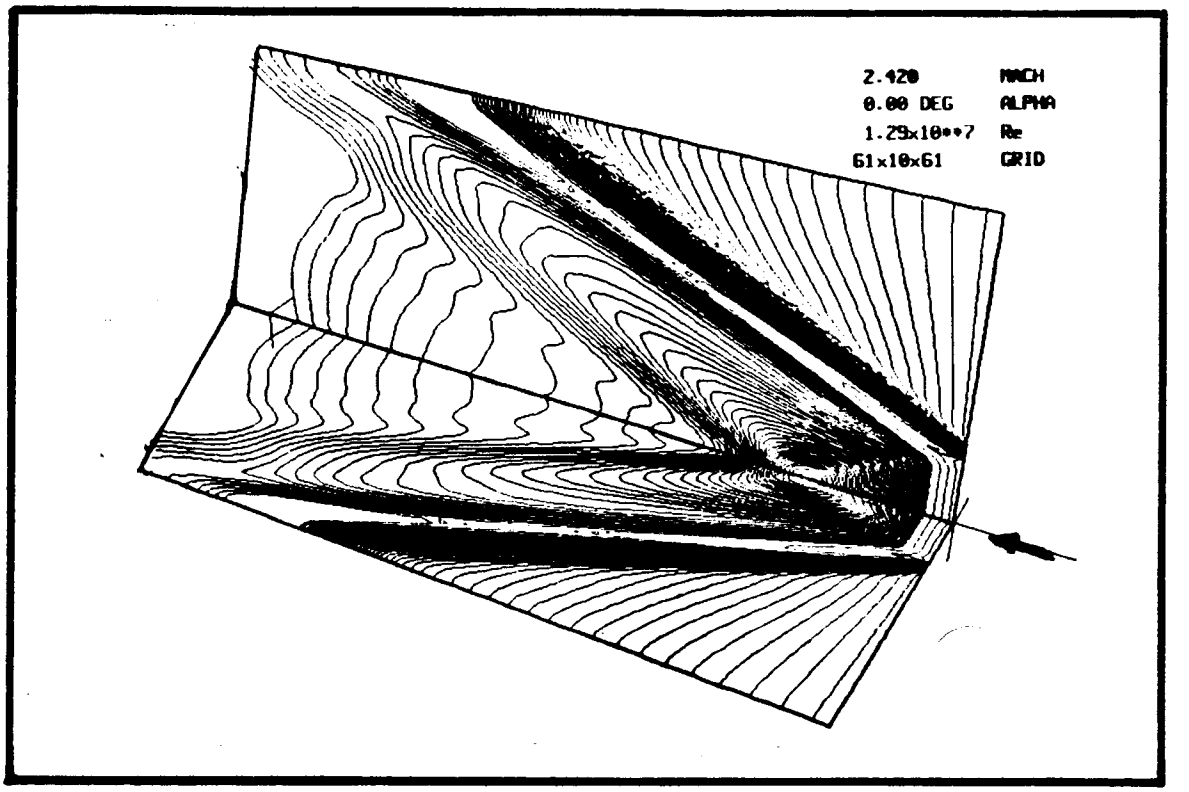

Figure 3. Pressure Contours - AGARD Test Case.

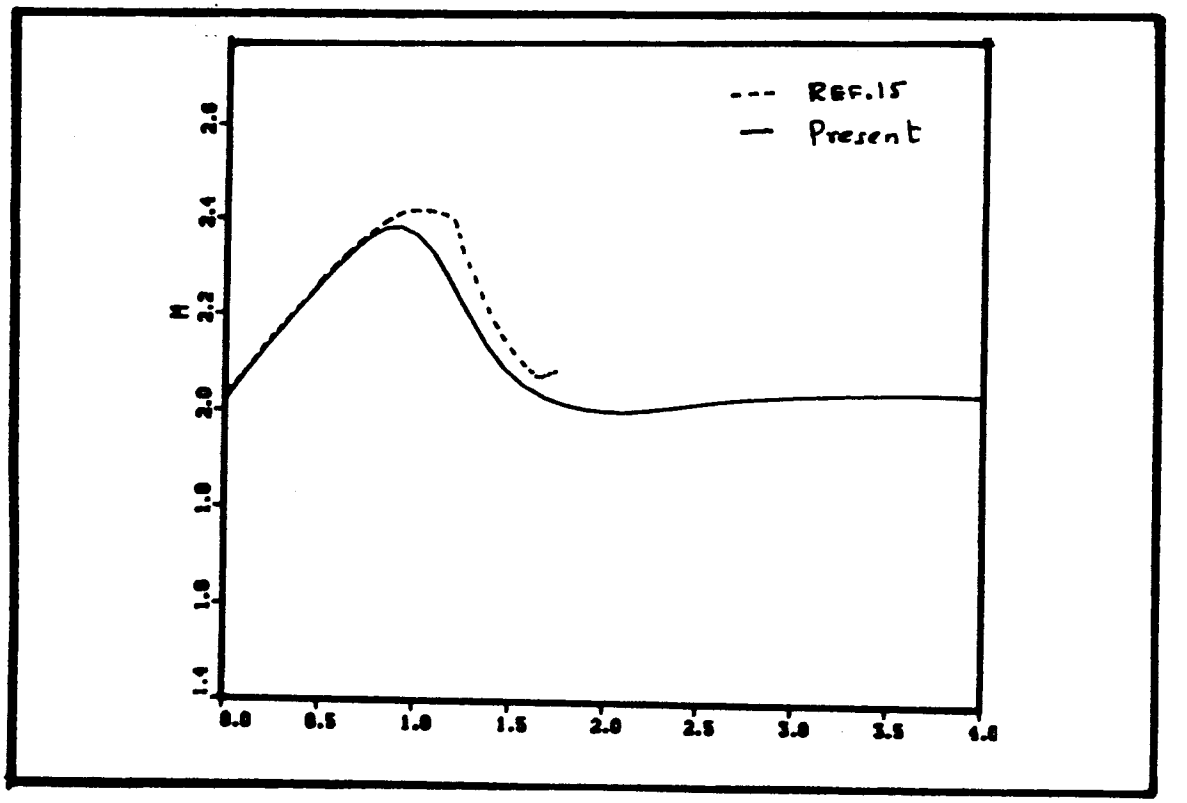

Figure 4. Mach Number Comparison Along the Jet Center Line.

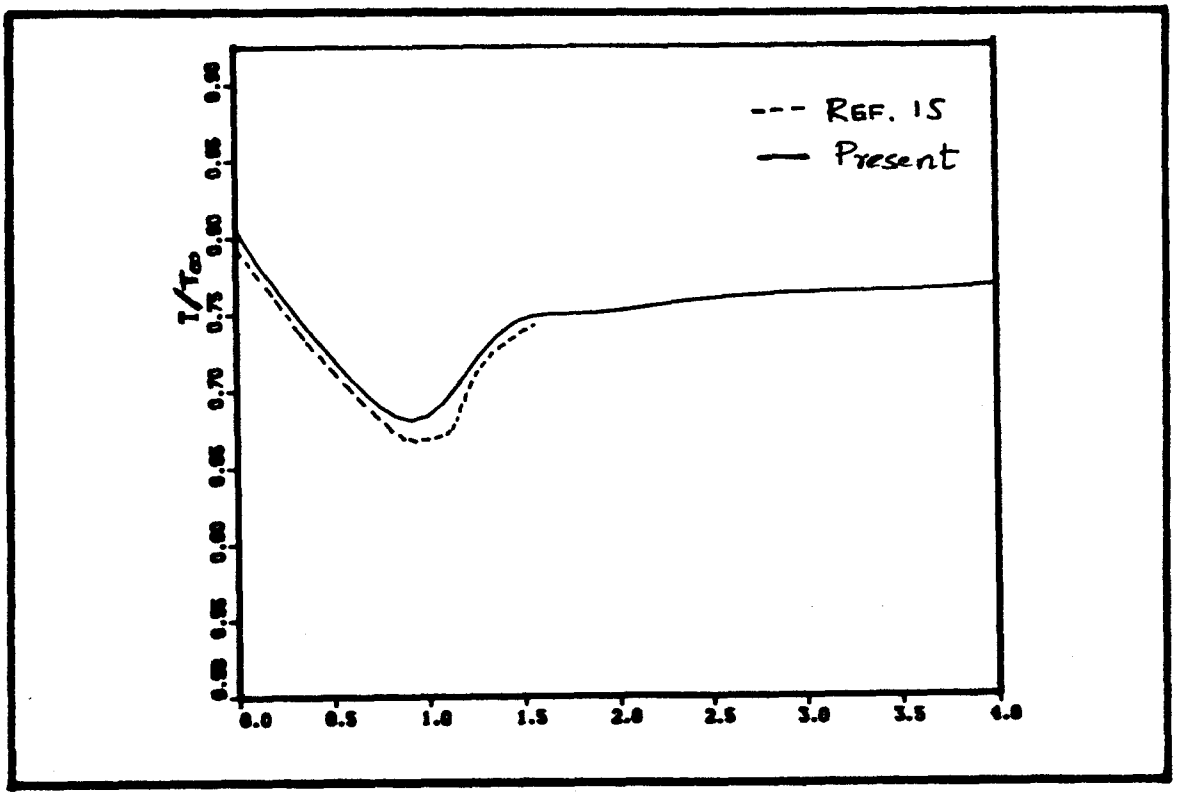

Figure 5. Temperature Comparison Along the Jet Center Line.

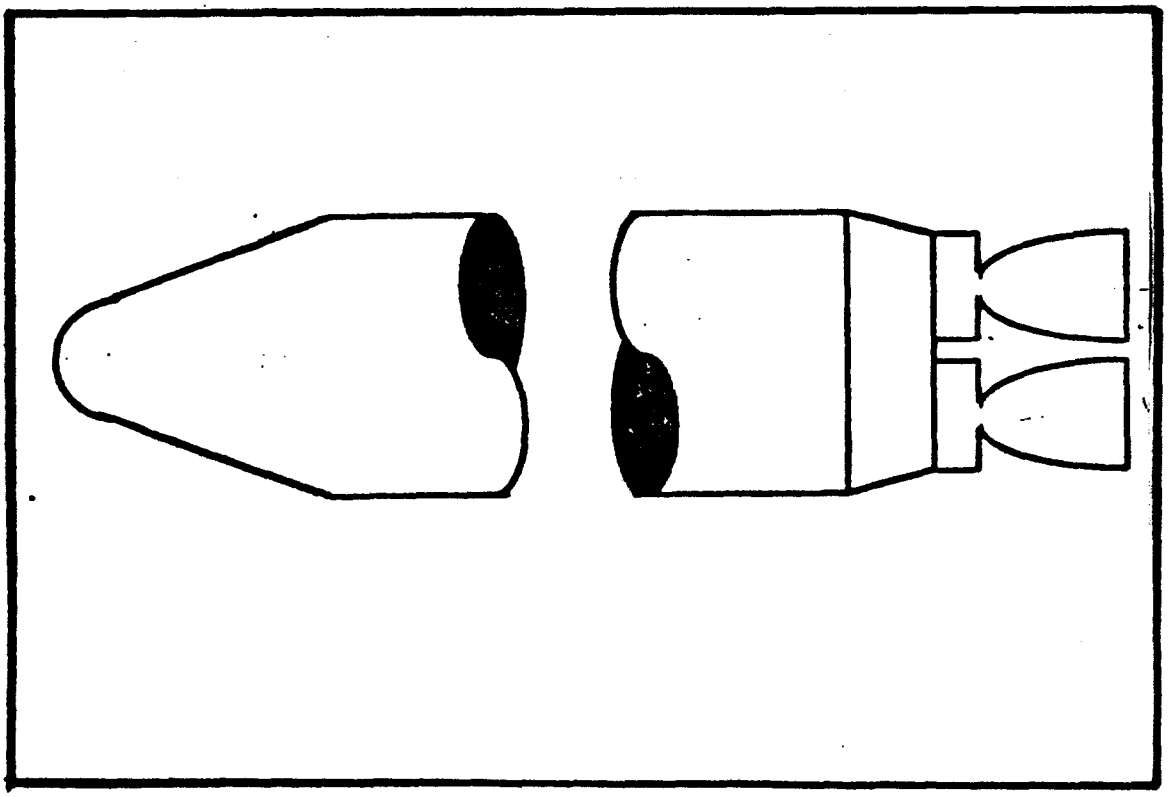

Figure 6. Generic Two-Nozzle Rocket Geometry.

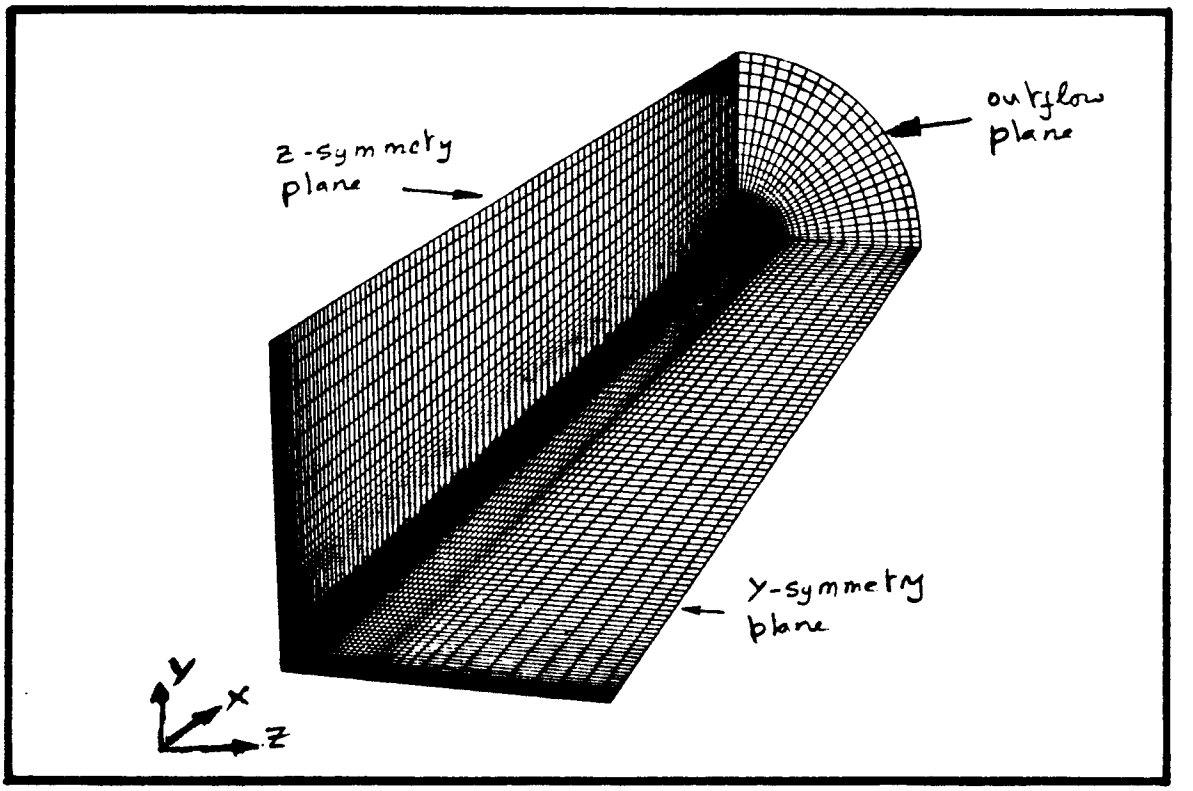

Figure 7. A 3-D Grid for the 2-Nozzle Plume Region

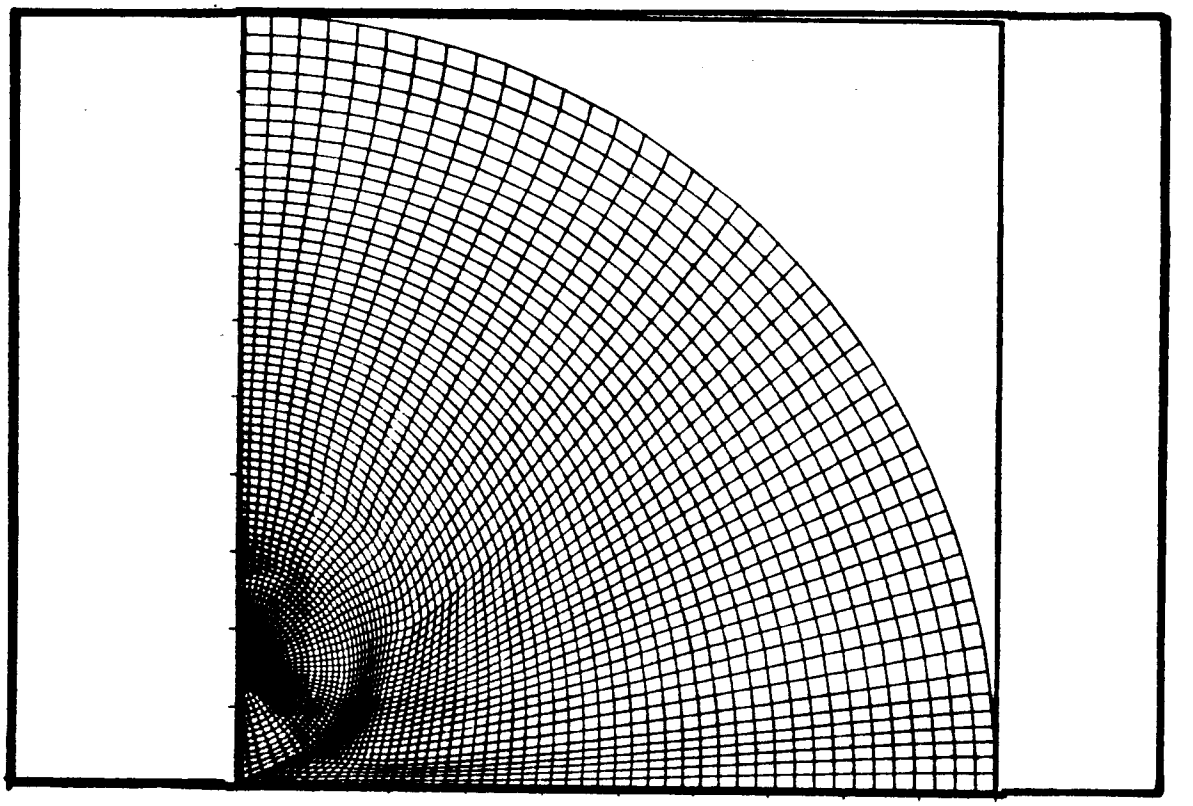

Figure 8. Grid Topology - X=constant Plane.

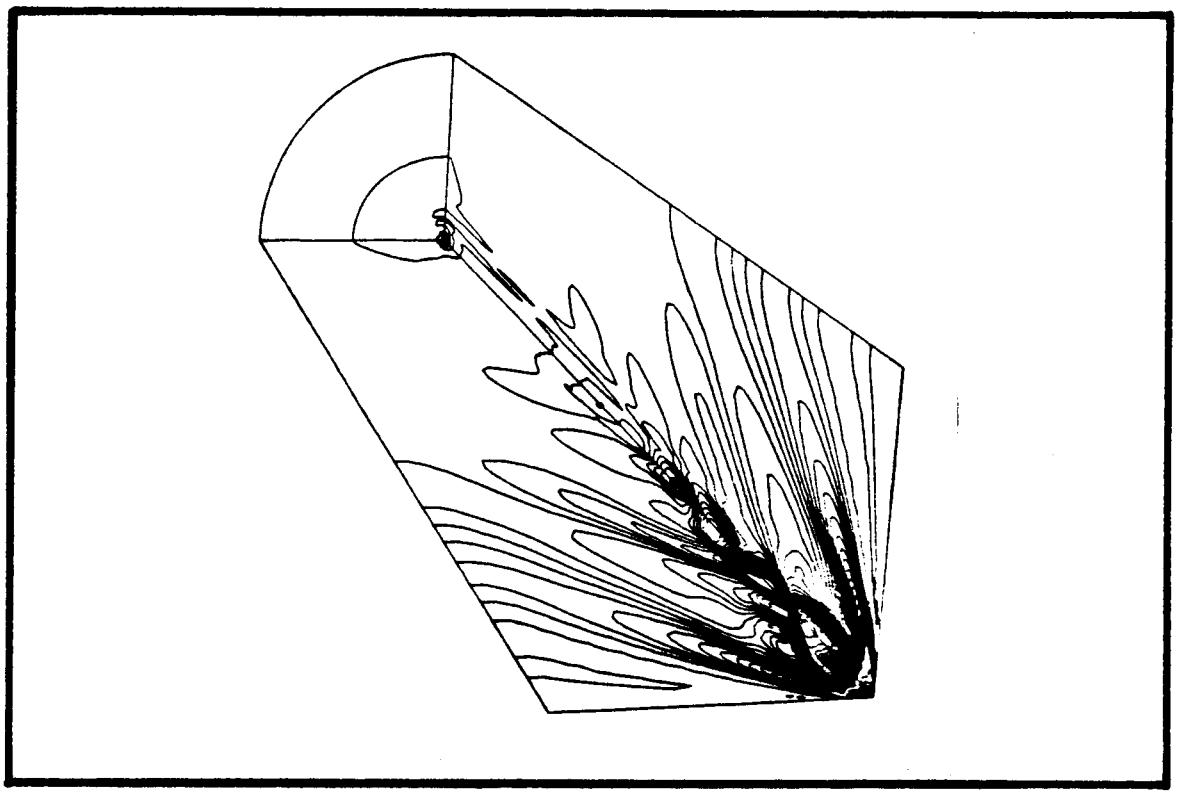

Figure 9. Pressure Contours - Test Case 1.

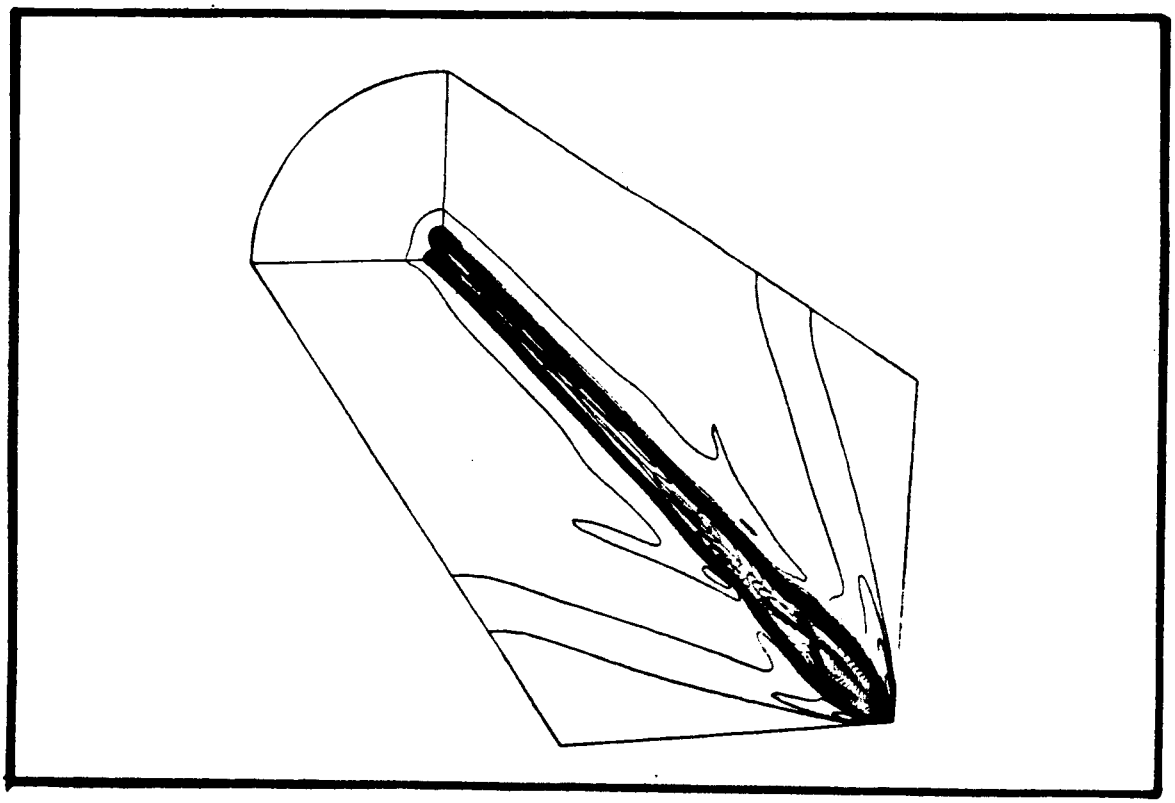

Figure 10. Mach Contours

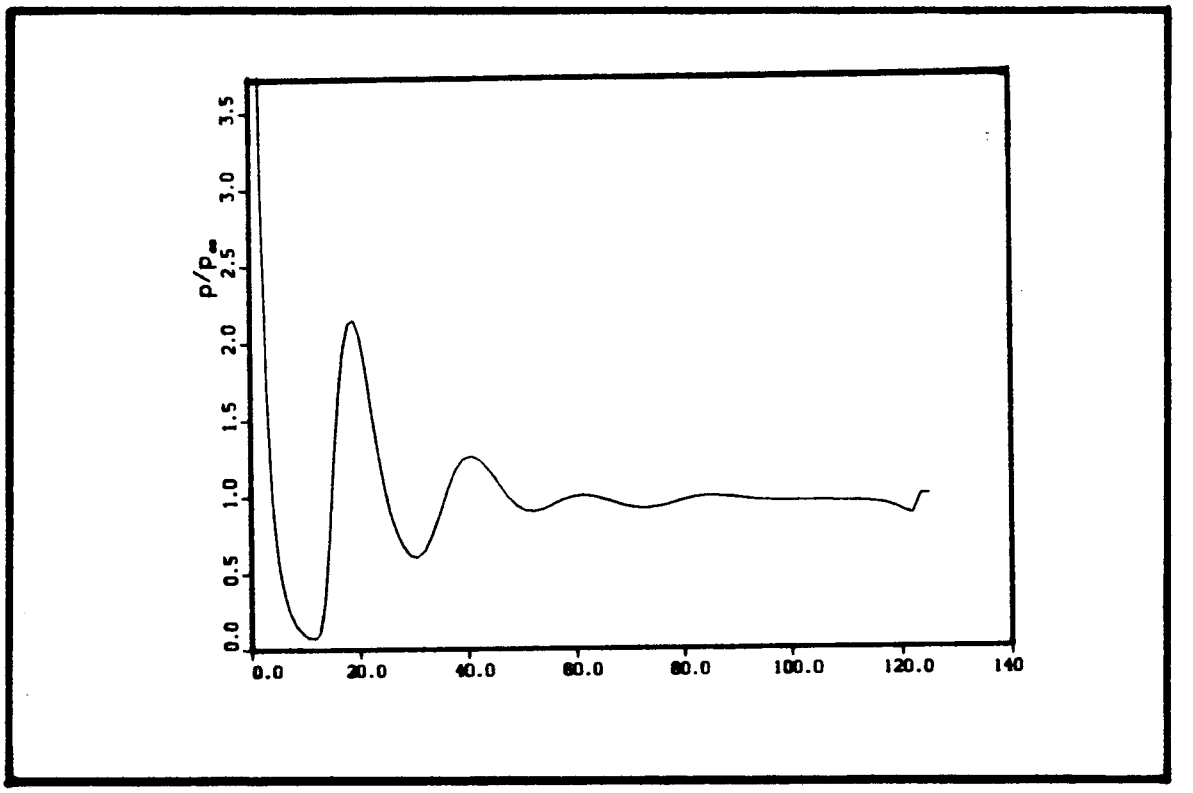

Figure 11. Normalized Pressure along X-axis - Test Case 1

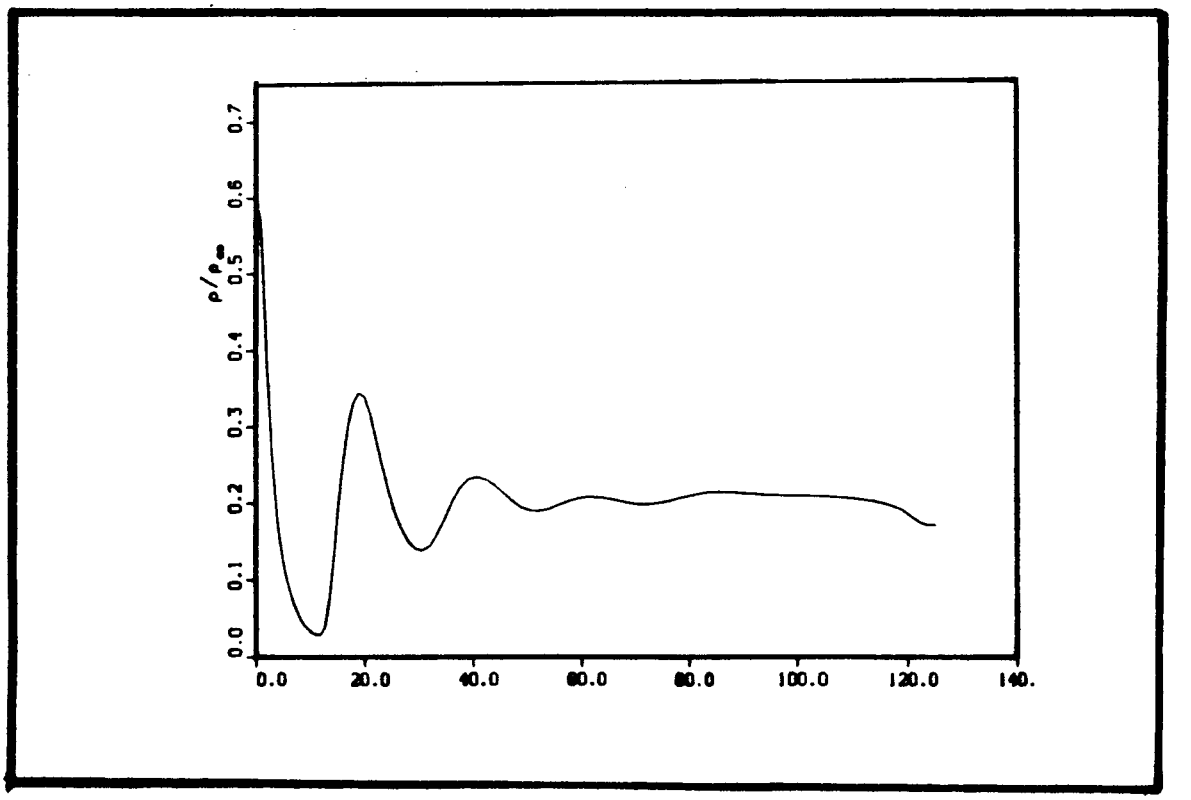

Figure 12. Normalized Density along X-axis - Test Case 1

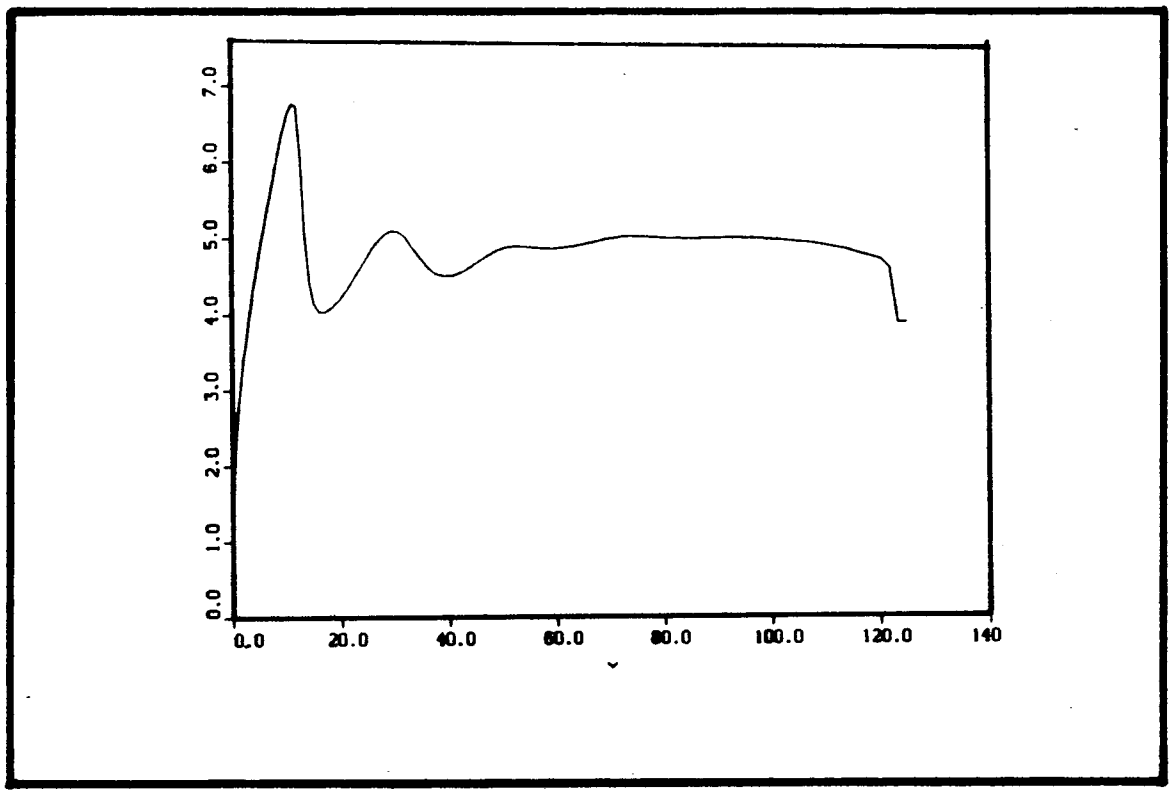

Figure 13. Normalized Mach Number along X-axis - Test Case 1.

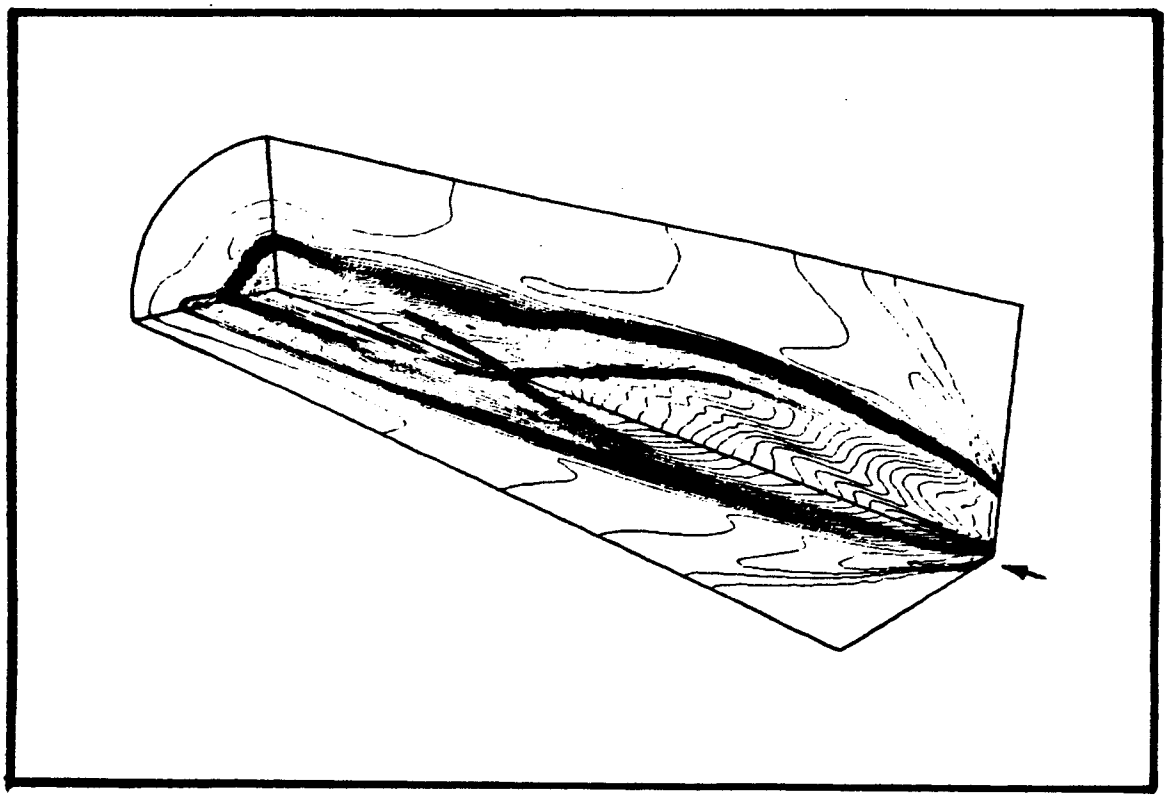

Figure 14. Mach Contours with Adapted Grid - Test Case 1.

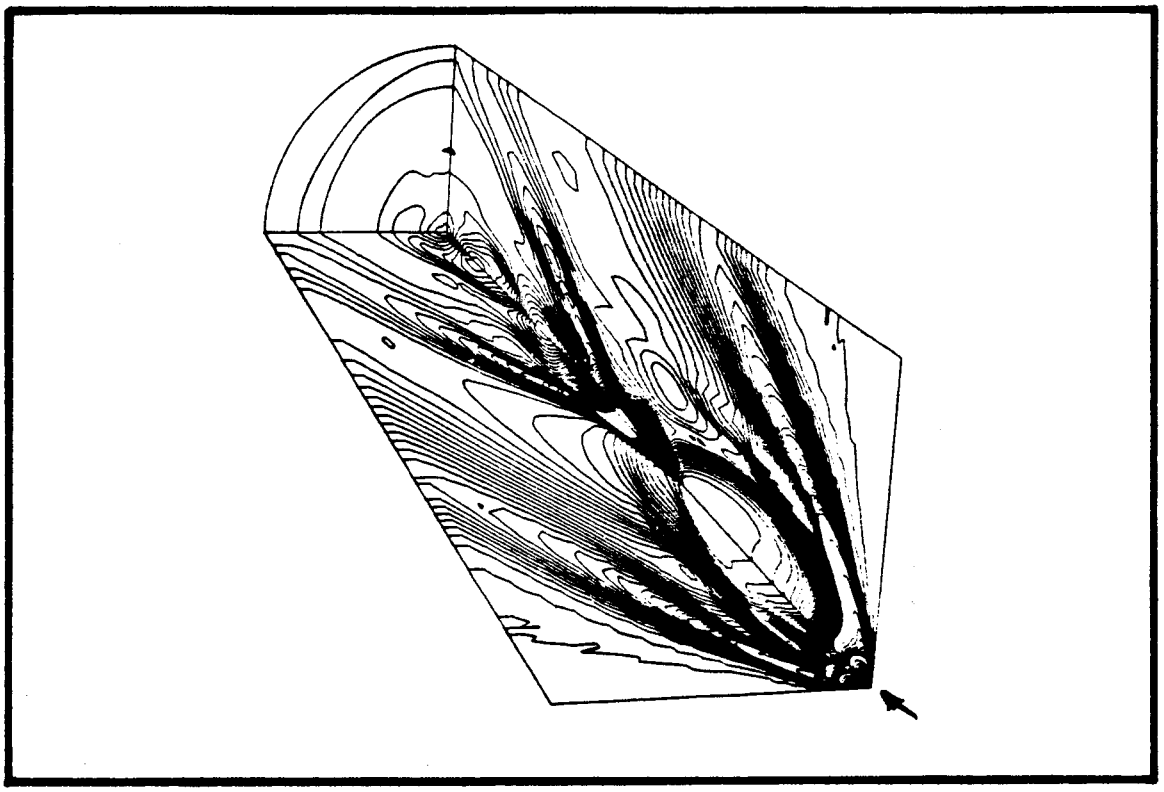

Figure 15. Pressure Contours - Test Case 2.

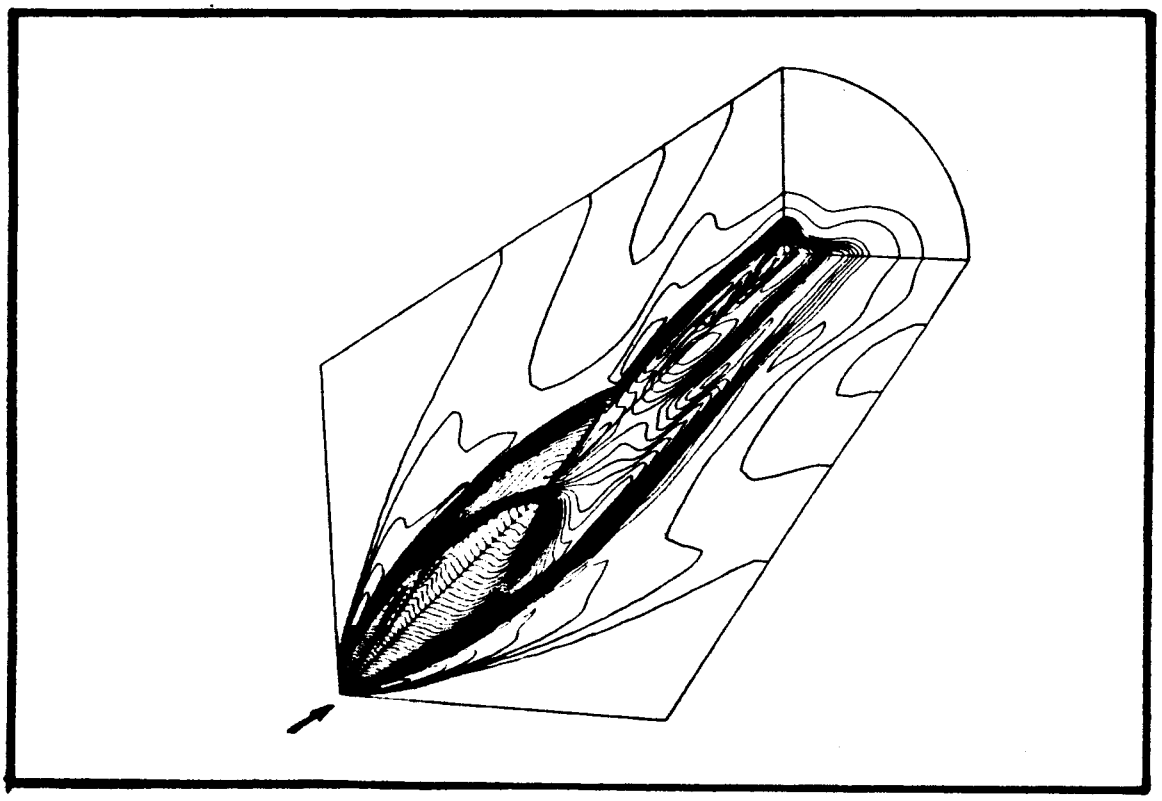

Figure 16. Mach Contours - Test Case 2.

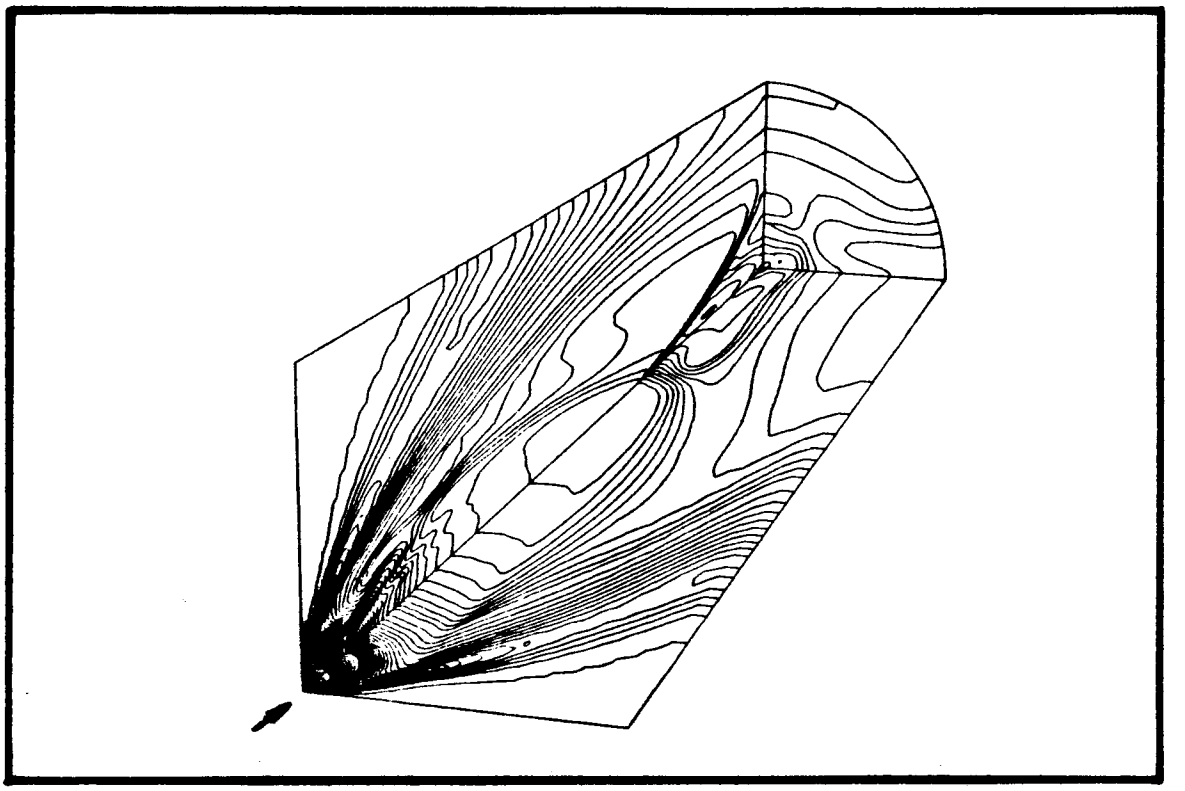

Figure 17. Pressure Contours - Test Case 3.

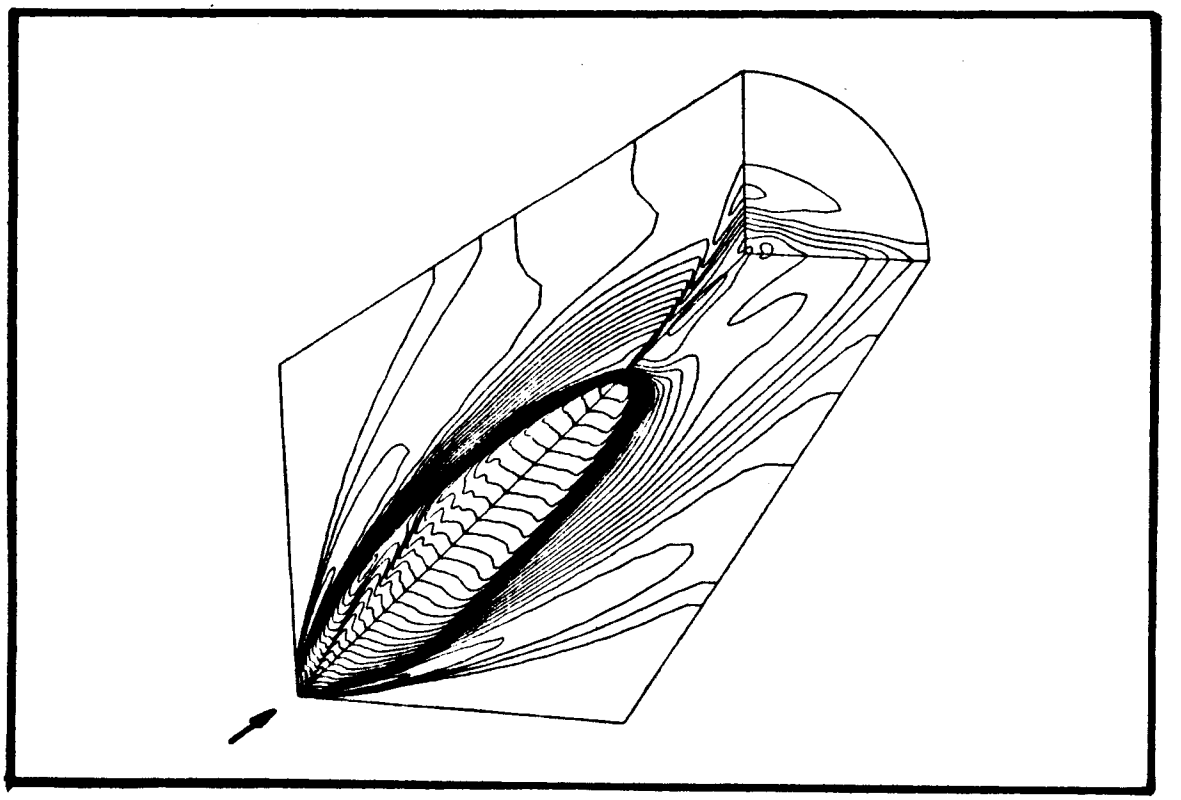

Figure 18. Mach Contours - Test Case 3.

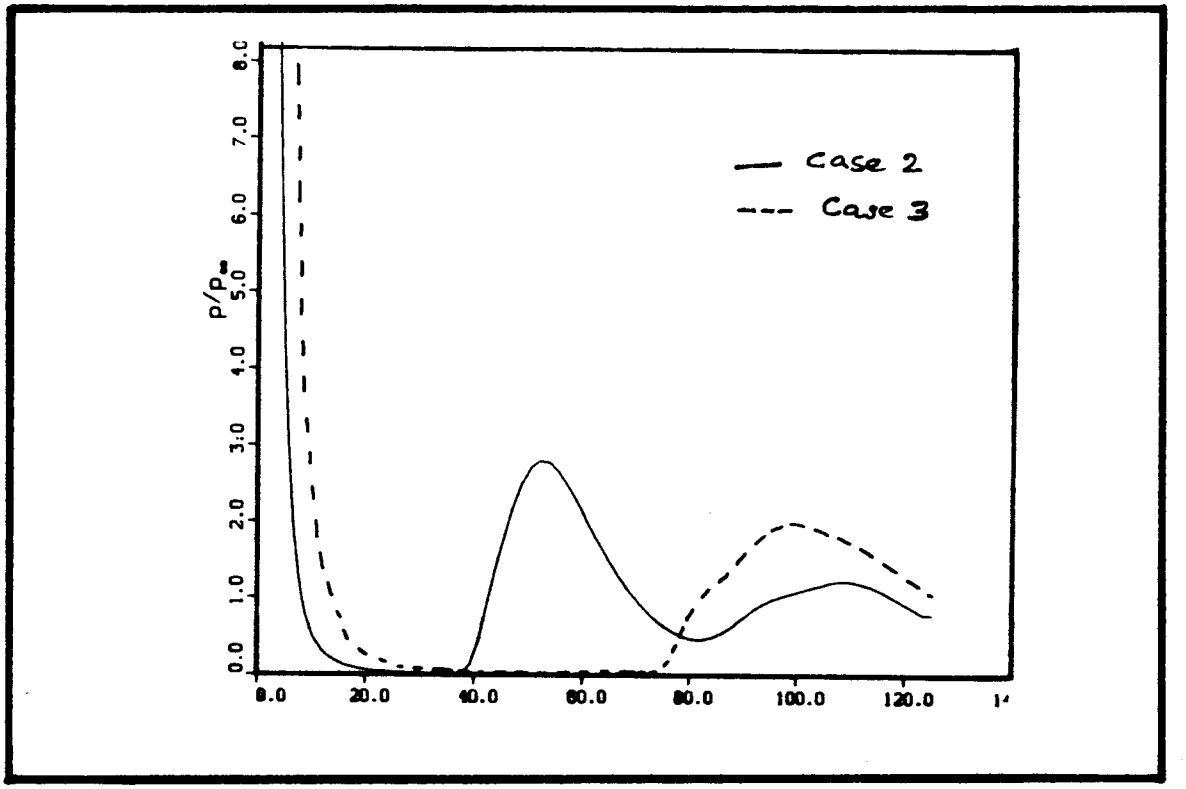

Figure 19. Pressure along X-axis - Case 2 and 3.

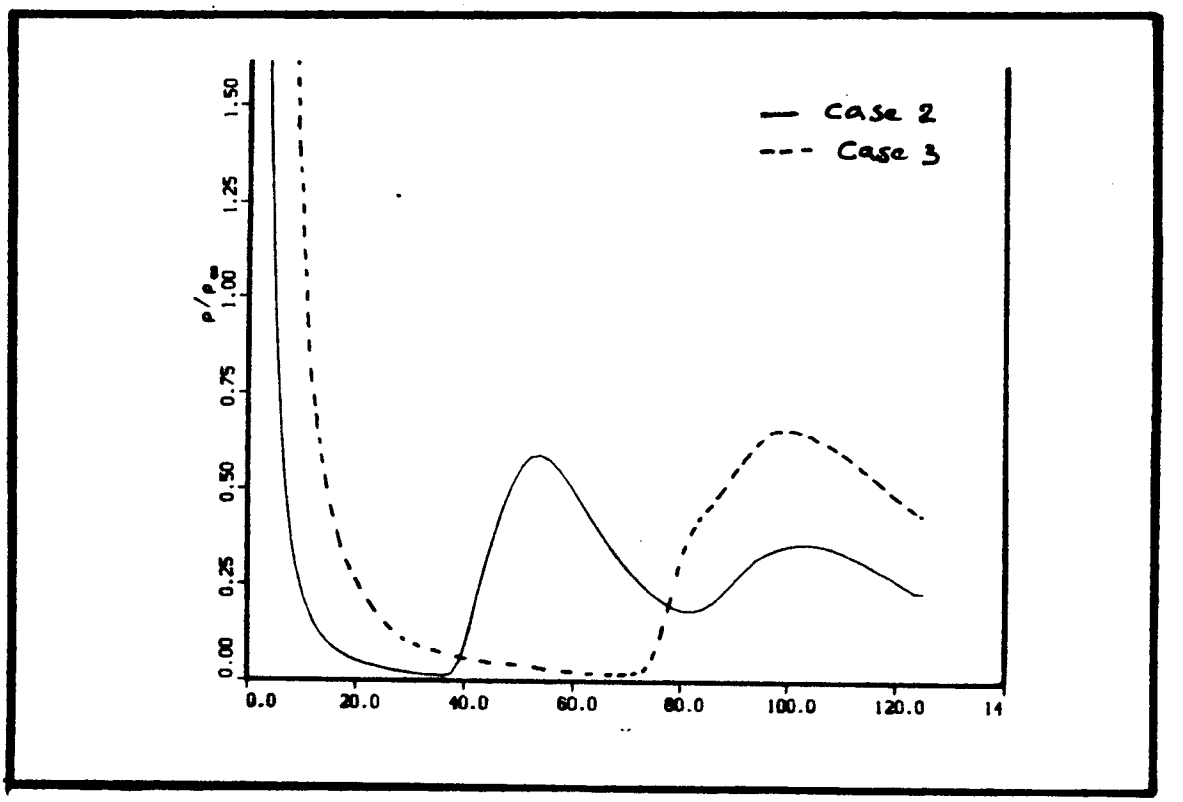

Figure 20. Density along X-axis - Case 2 and 3.

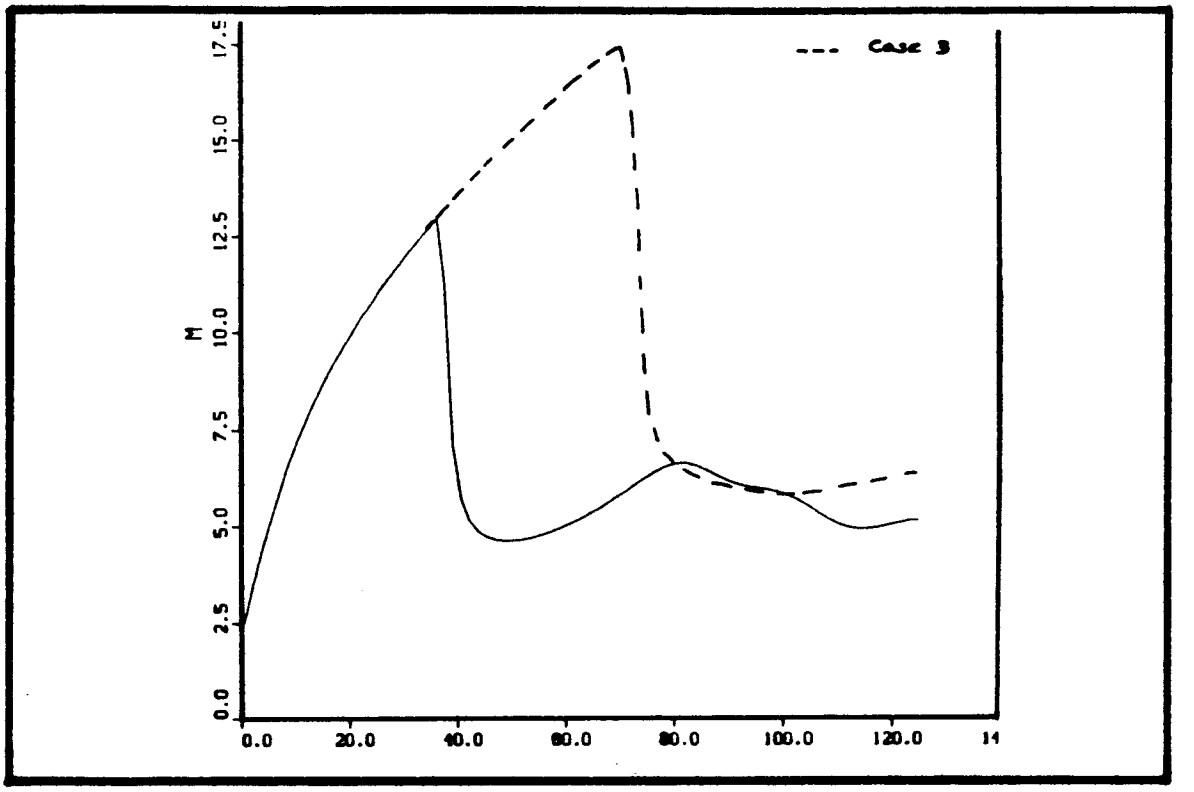

Figure 21. Mach Number along X-axis - Case 2 and 3.

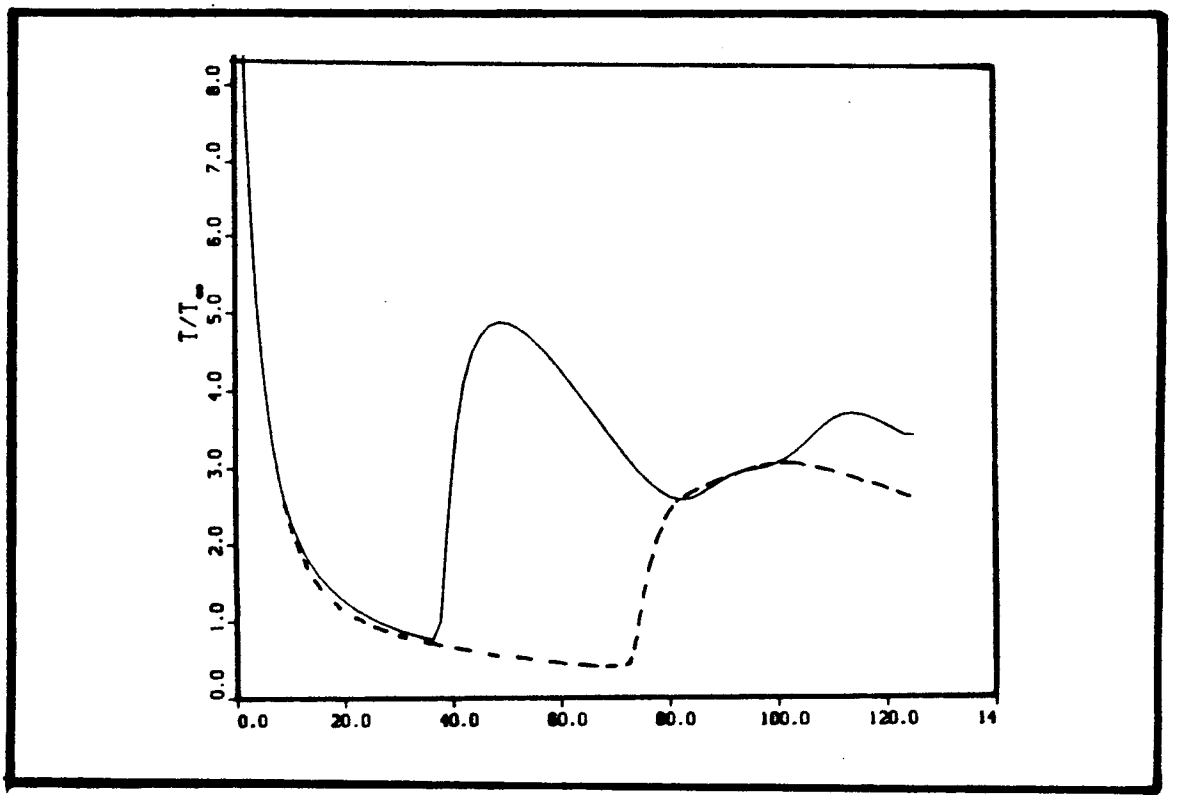

Figure 22. Temperature along X-axis - Case 2 and 3.